Biosensors and Bioelectronics 66 (2015) 69–76

Contents lists available at ScienceDirect

Biosensors and Bioelectronics

journal homepage: www.elsevier.com/locate/bios

Electrical impedance sensor for quantitative monitoring of infection processes on HCT-8 cells by the waterborne parasite *Cryptosporidium*

Alfred Dibao-Dina [a], Jérôme Follet [b,*], Mouhamad Ibrahim [a], Alexis Vlandas [a,**], Vincent Senez [a]

[a] Institut d'Electronique, de Microélectronique et de Nanotechnologie (IEMN), CNRS, UMR 8520, 59652 Villeneuve d'Ascq, France
[b] Laboratoire de Biotechnologies des Agents Pathogènes en Agriculture, Etablissement ISA groupe HEI-ISA-ISEN, 59046 Lille, France

ARTICLE INFO

Article history:
Received 1 September 2014
Received in revised form
28 October 2014
Accepted 6 November 2014
Available online 10 November 2014

Keywords:
Cryptosporidium
Infectivity
Bioimpedance
Cell-based assay
Quantitative monitoring

ABSTRACT

Cryptosporidium is the main origin of worldwide waterborne epidemic outbreaks caused by protozoan parasites. Its resilience to water chemical treatments and the absence of therapy led to consider it as a reference pathogen to assess water quality and as a possible bioterrorism agent. We here show that an electrical impedance-based device is able to get insights on *Cryptosporidium* development on a cell culture and to quantify sample infectivity. HCT-8 cells were grown to confluency on Interdigitated Microelectrode Arrays (IMA's) during 76 h and then infected by *Cryptosporidium parvum* during 60 h. The impedimetric response was measured at frequencies ranging from 100 Hz to 1 MHz and a 7 min sampling period. As the infection progresses the impedance signal shows a reproducible distinct succession of peaks at 12 h post infection (PI), 23 h PI and 31 h PI and local minima at 9 h PI, 19 h PI and 28 h PI. An equivalent circuit modeling-based approach indicates that these features are mostly originated from paracellular pathway modifications due to host–parasite interactions. Furthermore, our data present for the first time a real-time monitoring of early parasitic stage development with alternating zoite and meront predominances, observed respectively at peaks and local minima in the impedimetric signal. Finally, by quantifying the magnitude of the impedimetric response, we demonstrate this device can also be used as an infectivity sensor as early as 12 h PI thus being at least 6 times faster than other state of the art techniques.

1. Introduction

Cryptosporidium is a protozoan parasite which infects a wide range of vertebrates and more particularly human beings (Fayer, 2010). Between 2004 and 2010, 60% of worldwide reported outbreaks of diseases due to waterborne parasitic protozoa were *Cryptosporidium* induced (Baldursson and Karanis, 2011). Cryptosporidiosis outbreaks are present in both developing and industrialized countries (Chalmers, 2012) and can be lethal for immunocompromised or weak patients (Snelling et al., 2007). The largest outbreak took place in 1993 in Milwaukee (US), where 403,000 persons were affected and more than 100 died (Mac Kenzie et al., 1994). Furthermore, it has recently been shown that this pathogenic agent can induce gastrointestinal cancer in mice (Certad et al., 2007).

As no effective therapeutic treatment against the infection currently exists, tools allowing non-invasive and real-time analysis are needed to get a better understanding of the parasite infection processes.

Besides, the high resilience of the parasite to water chemical treatments such as chlorination (Cacciò and Pozio, 2006), the maintenance of its capacity to produce infectious forms, i.e. the infectivity, for more than 13 months (Chen et al., 2007) and the requirement of low inoculum to produce pathogenicity (less than 10 parasites) (Chappell et al., 2006; Okhuysen et al., 1999) lead also to consider this pathogen as a potential waterborne bioterrorism agent. As a consequence, it becomes essential to assess the risk with a rapid evaluation of sample infectivity. A common non-invasive electrical analysis on cell cultures is the so-called "TransEpithelial Electrical Resistance" (TEER). These systems deliver a burst of DC current through cells cultivated on a porous membrane at defined moments to determine cell layer permeability, mostly influenced by intercellular junctions (Ussing and Zerahn, 1951).

* Correspondence to: Laboratoire de Biotechnologies des Agents Pathogènes en Agriculture, Etablissement ISA groupe HEI-ISA-ISEN, 48 boulevard Vauban, 59046 Lille, France.
** Correspondence to: Institut d'Electronique, de Microélectronique et de Nanotechnologie (IEMN), CNRS, UMR 8520, BioMEMS, Avenue Poincaré, 59652 Villeneuve d'Ascq, France.
E-mail addresses: jerome.follet@isa-lille.fr (J. Follet), alexis.vlandas@iemn.univ-lille1.fr (A. Vlandas).

http://dx.doi.org/10.1016/j.bios.2014.11.009
0956-5663/

Some developments have been made to make similar measurements continuously, such as the CellZscope ® device (Wegener et al., 2004).

Impedance Spectroscopy (IS) is another common approach which displays several advantages: real-time monitoring, label-free analysis, high-throughput screening and ease of integration (Spegel et al., 2008). The combined use of IS and microelectrodes has demonstrated its usefulness in the field of cell biology. Pioneered by Giaever and Keese (1984) and adapted to Interdigitated Microelectrode Arrays (IMA) by Ehret et al. (1997), it has emerged as a powerful tool and been used to study a wide range of cellular phenomena such as cell adhesion and proliferation (Atienza et al., 2005; Wang et al., 2008; Wegener et al., 2000), cell confluency (De Blasio et al., 2004), cell apoptosis after chemical treatments (Arndt et al., 2004; Meissner et al., 2011; Solly et al., 2004) or stem cell differentiation (Bagnaninchi and Drummond, 2011). However, this technique has never been used either to get continuous information on the host cell response during protozoan parasite infection or to assess their infectivity. We here report that IS on IMA can be used to monitor in real-time the response of a cell culture infected by the waterborne parasite *Cryptosporidium parvum* (*C. parvum*). Furthermore, we show that the IS technique can provide insights on parasite development through their action on the cells which opens significant biological analysis opportunities. Finally, for the first time, we demonstrate that the infectivity of a parasite sample, i.e. its ability to produce infectious forms (King et al., 2012), can be measured and plotted as a dose response curve.

2. Material and methods

2.1. Biosensor fabrication

Inspired by a previously described protocole (Houssin et al., 2010), a square Pyrex substrate (5 cm × 5 cm × 0.7 mm thick) is first cleaned with a 5 min Piranha bath (1/3 H_2SO_4 in 2/3 H_2O_2), directly followed by Acetone and Isopropyl alcohol baths. Then, after a dehydration step, Dow ST hexamethyldisilazane (HMDS) is spin coated (2000 rpm, 1000 rpm/s, 20 s) to allow adhesion, again by spin coating, of AZ Electronic Materials AZ-nLOF 2020 photoresist (3000 rpm, 1,000 rpm/s, 20 s) afterwards. After a softbake step (110 °C, 1 min), 8 mm circular interdigitated round microelectrode arrays (with finger widths and gaps respectively of 100 μm and 7 μm in average) are patterned by UV-Lithography (I=53.9 mJ/cm²; postbake: 110 °C, 1 min) and developed with AZ Electronic Materials AZ MIF 326 (55 s) so that a titanium adhesive layer (10 nm) and gold (100 nm) can be deposited by evaporation. Lift-off is done using Dow ST SVC-14 solvent (70 °C, 40 min). Then, 6 mm wells are punched in 5 mm thick square-shaped polydimethylsiloxane (PDMS) and electrostatically fixed on the chip, which have been activated beforehand by Plasma O_2 (30 sccm, 150 W, 100 mT, 30 s) to improve the adherence. The well diameter is designed to be smaller than the IMA total area to ensure that the any cell growing at the bottom sits on the electrode and thus contribute to the signal. The microchip and its dimensions are presented in Fig. 1A and B. Finally, the chip is mounted on a home-made Printed Circuit Board (PCB). Previous to cell seeding, biosensor chips were sterilized with a 70% (vol/vol) alcohol treatment for 15 min at room temperature followed by three rinse steps with sterilized culture medium.

2.2. Cell culture

One standard method to evaluate *Cryptosporidium* infectivity is based on its development on cell cultures. HCT-8 cell lines (Human ileocecal adenocarcinoma, ECACC No 90032006) were maintained with regular subculturing in a growth medium consisting in a RPMI 1640 medium (Gibco, Invitrogen Corporation, France) supplemented with 1 mM Sodium Pyruvate, 2 mM L-glutamine, 10% (vol/vol) of heat inactivated fetal calf serum, 170 μM Streptomycin, 210 μM Gentamycin and Penicillin (100 U/L). Cells were grown in an incubator at 37 °C with 5% (vol/vol) CO_2 until monoloayers

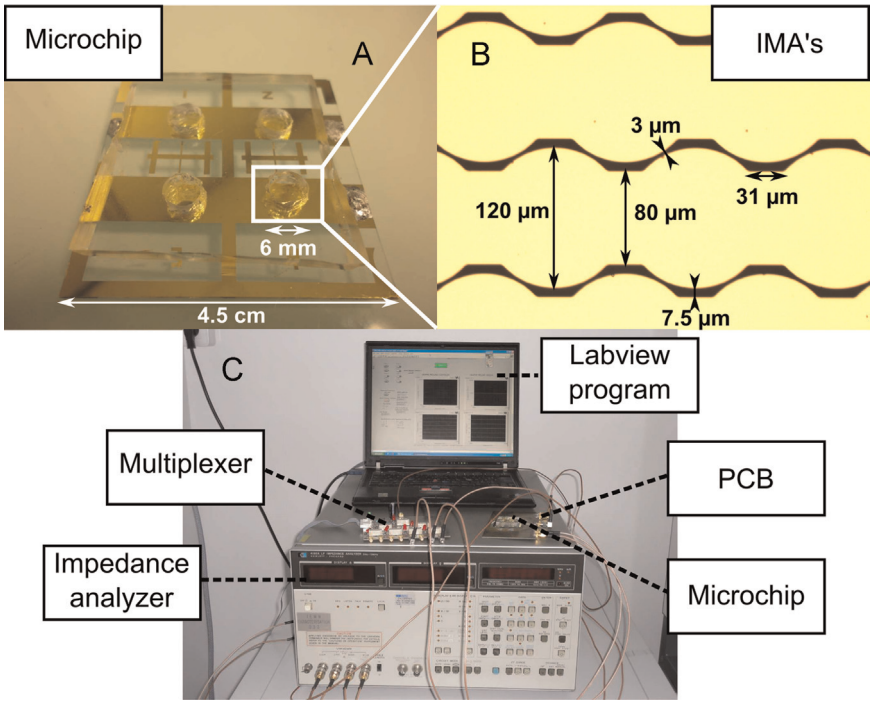

Fig. 1. Experimental set-up pictures. (A) Pictures of the whole setup, with the microchip mounted on a Printed Circuit Board (PCB) plugged with a multiplexer and a HP4192A impedance analyzer, driven by a Labview program. After cells or parasites were inoculated on the chip under a class 2 laminar flow hood, PCB and microchip were put in an incubator at 37 °C with 5% (vol/vol) CO_2. (B) Picture of the microchip, including 4 cell culture PDMS wells at the bottom of which Interdigitated Microelectrode Arrays (IMA's) were designed. (C) Picture of cells cultivated on IMA's. Average electrode width and gap are respectively 100 μm and 7.5 μm.

reached 80% confluency. Each well of the biosensor was seeded with 50,000 cells leading to a final number of 160,000 cells/well. At the same time, Lab-Tek™ Chamber Slides (Nunc™ International, Roskilde, Denmark) were seeded with the same number of cells. The biosensor and the Lab-Tek™ chamber slides were incubated during 76 h before infection.

2.3. Oocyst and inoculum preparation

C. parvum oocysts of "Iowa" strain were purchased from Waterborne Inc. and stored in phosphate buffer salin (PBS) at 4 °C. Prior to any experimentation, excystation rates were determined for each batch using a standard procedure. Briefly, oocysts were incubated for 1 h at 37 °C in PBS complemented with 0.25% (wt/vol) trypsin and 0.75% (wt/vol) taurocholic acid. Afterwards, the oocyst suspension was placed on a glass slide, coverslipped and viewed under DIC optics (Nomarski) with a Nikon 80i microscope (Nikon, Tokyo, Japan) at 630 × magnification. Percentage of excystation was determined by counting 500 events corresponding to intact or empty oocysts (ghosts). Excystation rate was calculated using the equation: (number of empty oocysts/total of intact and empty oocysts) 100 ×. Only oocyst batches exhibiting excystation rates greater than 70% were used for our experiments.

In order to standardize the procedure of infection, all inocula were done so that a [viable sporozoite]:[cultivated cell] ratio of 1:1 would correspond to the presence of one sporozoite released per HCT-8 cell settled in the device. Number of oocysts in the inoculum of 1:1 was then determined as: ((number of HCT-8 cells/4)/excystation rate) 100 ×. As a negative control (0:1), a pool containing the same amount of oocysts was inactivated by 2 steps of freezing in liquid nitrogen for 1 min and thawing at 37 °C for 1 min. In order to see the influence of the [viable sporozoite]:[cultivated cell] ratios on the impedimetric response, we designed ratios of 1:2 and 1:4 by mixing pristine and inactivated pools of parasites. We however kept the total number of introduced oocysts to ensure changes do not originate from a change of this parameter.

2.4. Infection protocol

According to the infectivity assay developed by Keegan et al. (2003), after a washing step by centrifugation at 1800 g for 20 min at room temperature, oocysts were incubated in acidified water (pH 2.4) containing 0.025% (wt/vol) of trypsin, at 37 °C for 20 min, to trigger excystation. After a second centrifugation step at 1800 g for 10 min, oocysts were suspended in a maintenance medium. The maintenance medium consisted of RPMI 1640 medium with 2 mM L-glutamine, 15 mM HEPES buffer, 23 mM sodium bicarbonate, 5 mM glucose, 0.5 μM folic acid, 7 μM 4-amino-benzoic acid, 0.1 μM calcium pantothenate, 50 nM ascorbic acid, 1% (vol/vol) heat inactivated fetal calf serum, 210 μM gentamycin, 170 μM streptomycin and penicillin (105 U/L). Before oocyst inoculation, growth medium was switched with maintenance medium. Triggered oocysts were finally added on monolayers and the culture systems were incubated during 60 h at 37 °C in 5% (vol/vol) CO_2 atmosphere. During the whole process, in order to prevent bacterial contaminations, all solutions were filtered beforehand at 0.22 μm. Their absence was insured by testing solutions and supernatants of culture at 37 °C overnight on a Plate Count Agar growth medium in Petri dishes after each manipulation of the process and at the end of the experiment.

The sensitive layer, i.e. the HCT-8 cells layer, has been used for only one infection protocol in this study before being regrown. Indeed, it was feared that the stress induced by the first experiment might have affected cell response if they had not been renewed and thus compromised the reproducibility of our results. However, the microchip itself has been re-used for up to three experiments (after a cleaning procedure) while providing a good reproducibility. This was studied by measuring the microchips impedimetric properties after each cleaning round. These consisted of a first step during which the wells were rinsed with Mili-Q water to remove the cells and the parasites, followed by 3 steps of with a 70% (vol/vol) alcohol treatment.

2.5. Electrical impedance measurements

Real-time cell layer impedance measurements were successively made on each well using an impedance analyzer (Agilent HP 4192A) and a home-made multiplexer, both linked to the PCB with SMA cables. A Labview program monitored both the impedance analyzer, to automatically perform and record the impedance measurements for a defined well at 10 mV for 81 frequencies ranging from 100 Hz to 1 MHz, and the multiplexer, to perform cyclic changes of the recorded well after measurements for all frequencies (see Fig. 1C). Seven minutes separate the recorded data for one well at a defined frequency. These measurements were continuously performed during 136 h, with a short break at 76 h corresponding to the oocyst insertion. Finally, data for each well as a function of time were extracted with a Matlab program.

2.6. Equivalent circuit modeling

In order to put hypotheses on biological processes explaining the global impedimetric response of the 1:1 ratio we isolated its various contributions with an equivalent circuit modeling. The circuit, schematized in Fig. 2A and B, was inspired by a previously used lumped circuit (Meissner et al., 2011). The ionic double layer is modeled by a constant-phase element (CPE, see Eq. (1)), an element with a frequency-independent phase angle between 0° and 90° and 2 parameters P and n:

$$Z_{CPE} = \frac{1}{P(j\omega)^n} \tag{1}$$

where j stands for the imaginary number ($j^2 = -1$) and ω for the radial frequency (rad/s). Although an ideal double layer can be modeled with a capacitance, it often reveals in practice a phase angle slightly inferior to 90°, mostly explained by electrode

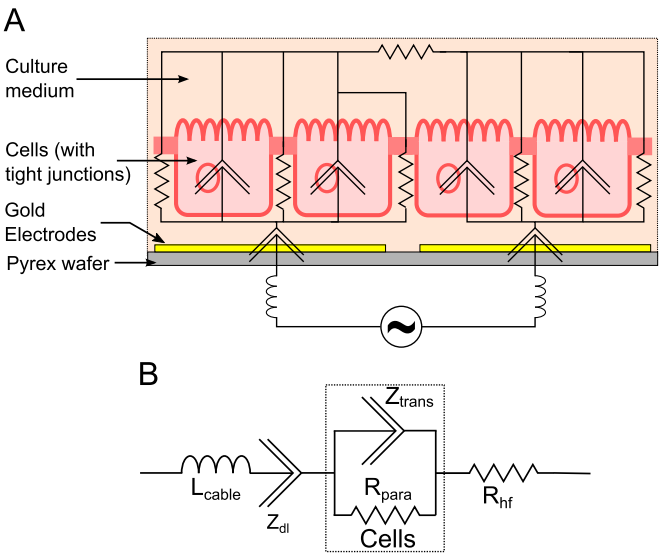

Fig. 2. Modeling with an equivalent circuit. (A) Schematic of the equivalent circuit. At the cell layer, transcellular pathways are modeled as a CPE and paracellular ones as a resistance. (B) Simplified equivalent circuit, which fittings are based on. (C) Time-course of R_{para}, P_{trans} and n_{trans} compared to total impedance at 5 kHz.

roughness (De Levie, 1965) and specific protein adsorption (McAdams et al., 1995). CPE are used in such typical cases (Jorcin et al., 2006).

The high frequency range (between 100 kHz and 1 MHz) is dominated by set-up inductances and lead and bulk medium resistive effects. At the chosen frequencies, the capacitive component of the culture medium, highly conductive, is invisible and thus not represented (Houssin et al., 2010). Single cells are generally represented with a resistance, to represent the paracellular pathway, in parallel to a capacitance in series with a resistance, both respectively representing the cell membrane and the cytoplasm, i.e. the transcellular pathway. As the cytoplasm is as conductive as the bulk medium, it is here negligible thus the resistance is not modeled. However, cell layers are highly heterogenic in terms of cell size and shape and locally present various time constants, inducing a distribution of relaxation times (Schwan, 1985). This leads to a non-ideal capacitance behavior of the transcellular pathway, which can as well be modeled with a CPE (Cole and Cole, 1941).

The impedance of a cell layer infected by a [viable sporozoite]: [cultivated cell] ratio of 1:1 has been fitted to the described equivalent circuit over the infection time, i.e. 60 h, with the freely available software EIS spectrum analyzer (Pomerantsev, 2005). To improve the reliability of the fitted parameters, each data point has been fitted with a weighted determination coefficient r^2 equal to at least 0.999, calculated by the software following the Eq. (2):

$$r^2 = 1 - \left(\frac{1}{n-p} \sum_{i=1}^{N} \frac{(Z'_{meas} - Z'_{fit})^2 + \left(Z''_{meas} - Z''_{fit}\right)^2}{\left(Z''_{meas} - Z''_{meas}\right)^2} \right) \quad (2)$$

Z'_{meas}, Z''_{meas}, Z'_{fit} and Z''_{fit} are respectively the real and imaginary part of the measured and the calculated impedance, n is the number of fitted points, i.e. 81 between 100 Hz and 1 Mhz, and p the number of parameters of the equivalent circuit.

2.7. Fluorescence staining

Further explanations of the impedimetric response required information on parasite developmental forms and cell layer coverage. Both analyses can be performed by fluorescence microscopy. However, this approach requires a chemical fixation step of the cells previous to immunolabeling. As this step kills cells, it cannot be done directly in the chip wells. As a solution, we cultured and infected HCT-8 cells in Lab-Tek™ Chamber Slides at the same time as in the microchip, which allowed us to identify and quantify parasite developmental forms and the cell layer coverage. After aspiration of the supernatant from the Nunc™ Lab-Tek™ Chamber slide wells, cells were rinsed with Hanks Balanced Sodium Salt (HBSS, Gibco® life technologies ™ UK). A fixation step was then performed using 4% Formaldehyde during 15 min in a humid atmosphere at 37 °C. Before each labeling, cells were rinsed 3 times with HBSS and 1 time afterwards. *Cryptosporidium* developmental forms were labeled with a polyclonal IgG antibodies reaction kit tagged with fluorescein (FL-Crypt-a-Glo™ Kit, Waterborne Inc., New Orleans, LA, USA). Antibodies were 1/20th diluted and incubated on cells for 1 h at 37 °C. Cell membrane were labeled with a Wheat Germ Agglutinin Alexa Fluor® 555 conjugate (Invitrogen, UK) for 20 min at room temperature. DNA was labeled with 4′.6′-diamidino-2-phenylindol (DAPI) for 2 min at room temperature. Slides were then coverslip with a no fading mounting medium (Waterborne Inc. New Orleans, LA, USA) and observed with a Nikon 80i microscope. Pictures were captured with a Nikon DXM 1200C digital camera and treated with NIS-Elements Microscope software (Nikon, Tokyo, Japan).

2.8. Fluorescence observation

The observations were performed at 9 specific moments corresponding to peaks, local minima and final impedance drop of the 1:1 impedance time-course post infection. They were determined by averaging time points on 3 former measurements and running simultaneously an infected cell layer impedance well. Cell coverage and parasites were observed using Differential Interference Contrast (DIC) and fluorescence microscopy on a representative number of fields as described in Fig. S1. The recorded parasitic forms were grouped in three categories, depending on their size and their number of nuclei: zoites, i.e. mononucleated structures ranging from 1 μm to 4 μm corresponding to the invasive forms (sporozoite, trophozoite, merozoite); meronts, i.e. bigger multinucleated (4–8 nuclei) structures ranging from 3 μm to 5 μm corresponding to proliferating forms (type I and II meront); gamonts, i.e. wider multinucleated (14–16 nuclei) forms ranging from 3 μm to 6 μm, associated to sexual reproduction (micro and macrogamont). These structures have been precisely described by Hijjawi et al. (2001) and Slifko et al. (1997) and examples of them can be found in the Supplementary Information (Fig. S2). Average and standard deviations were made on 3 wells.

2.9. Data interpretation and statistics

For each group of parasite infection and negative control, the mean value and SD were calculated at each time point. For the sake of visibility error bars were plotted every 10 points. All experiments were done at least 3 times on different devices. ANOVA tests were performed to determine significant difference between groups.

3. Results

3.1. Specific host cell impedimetric response to C. parvum infection

Cryptosporidium persists in the environment as resilient oocysts. Upon ingestion, 4 sporozoites are excysted from this oocyst in the gastrointestinal tract where they infect lumen cells. HCT-8 (Human Colon Carcinoma cell line) cell lines have been chosen as model for the gastrointestinal tract as they display optimal sensitivity to *C. parvum* infection (Upton et al., 1994). HCT-8 cells have first been cultivated on IMA and their impedance continuously recorded during 76 h at frequencies from 100 Hz to 1 MHz with a 7-min sampling period (Fig. S3A). *C. parvum* samples containing a ratio of 1 sporozoite per cell (1:1) and 1 freeze-and-thaw inactivated sporozoite per cell (0:1, negative control=fully inactivated sample) were added to the culture chamber. This step establishes the time reference noted 0 h post infection (0 h PI) as the impedance was recorded during 60 h (Fig. S3B).

For frequencies between 1 kHz and 100 kHz, 3 stages can be distinguished (Fig. 3). For the first stage ranging from the inoculation time point to 9 h PI, no significant difference was observed. During the second stage ranging from 9 h PI to 40 h PI, the impedance was higher than the control and displays three peaks at 12 h PI, 23 h PI and 31 h PI and 3 local minima respectively at 9 h PI, 19 h PI and 28 h PI. The third stage ranged from the time point where the curve passes under the control, which is frequency-dependent, until the end of the experiment.

3.2. Cell layer analysis by equivalent circuit

As the response of our system is frequency-dependent, we rely on an equivalent circuit analysis, schematized in Fig. 2A. The modeling was based on the simplified circuit shown in Fig. 2B. The

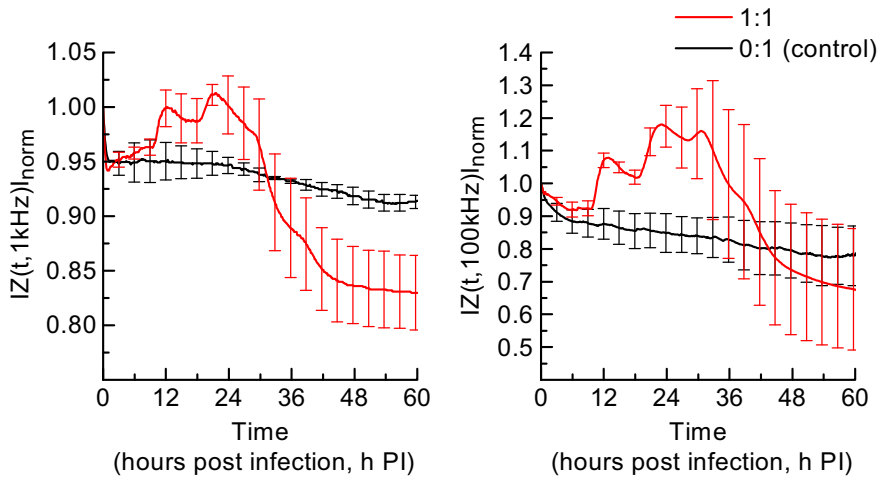

Fig. 3. Real-time monitoring of *Cryptosporidium* infection of confluent HCT-8 cell layer during 60 h (PI=post infection). Time-course of the cell layer normalized impedance magnitude $|Z(t,f)|_{norm}$ is represented at 1 and 100 kHz. Cells were infected with a ratio of 1 viable sporozoite per cultivated cell (ratio 1:1) or with sporozoites inactivated by a freezing-and-thawing step (0:1 ratio, negative control). Values are mean ± SD, $n=3$.

values were fitted for each electrical component as a function of time (see Table S1 and Fig. S2). The three components related to the cell layer namely R_{para} for the paracellular electrical path, P_{trans} and n_{trans} for the transcellular path, are plotted in Fig. 4. At 5 kHz, para- and trans-cellular pathways are almost equally weighted (Fig. S4), thus we chose this frequency to compare the total impedance to cell parameters.

While R_{para} closely follows time-course impedance shape, as the 3 stages previously described can be observed again, P_{trans} and n_{trans} evolution are quite different. Between 0 and 19 h PI, P_{trans} remains stable while n_{trans} and impedance slopes are opposite. Then, P_{trans} starts to increase to values five times higher than the initial ones until 45 h PI before it slowly decreases until the end of the experiment. On the other hand, n_{trans} first decreases from 19 h PI to 32 h PI and then gradually increases from 32 h PI to 60 h PI.

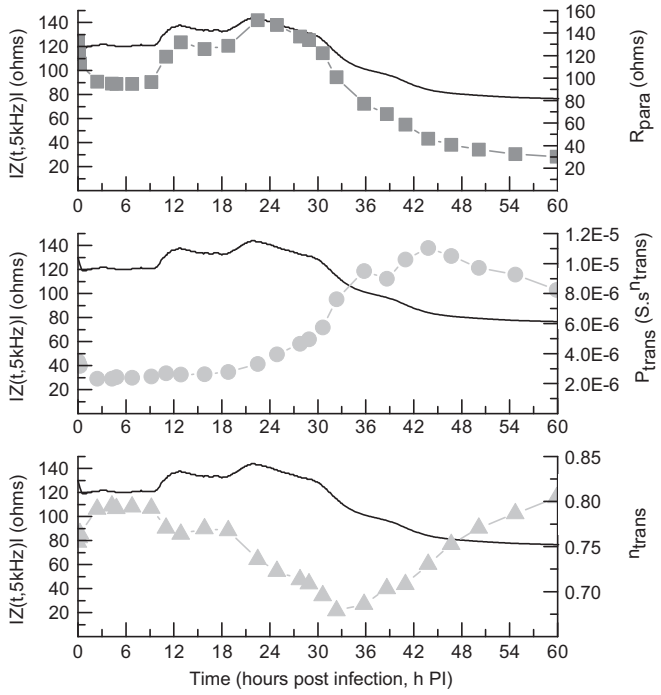

Fig. 4. Time-course of R_{para}, P_{trans} and n_{trans} compared to total impedance at 5 kHz at a [viable sporozoite]:[cultivated cell] ratio of 1:1.

3.3. Alternation of zoite and meront predominances

In order to quantify parasite proliferation and forms during the infection, several Labtek™ chamber slide wells were exposed to our 1:1 [viable sporozoite]:[cultivated cell] ratio protocol and the parasitic developmental forms were counted on a representative number of fields. These countings were performed at 9 specific moments corresponding to peaks, local minima and final impedance drop. These forms were grouped in three classes: zoites (asexual mononucleate), meronts (asexual multinucleate) and gamonts (sexual multinucleate).

Our data show that the total parasite number increases until 39 h PI before displaying a slight decrease at the end of the experiment (Fig. 5A). Zoite and meront predominances successively alternate from 4 h PI to 30 h PI (Fig. 5B). These zoite and meront predominances were respectively consistent with impedance peaks and local minima. This microscopy analysis also detected the appearance of the first gamonts at 39 h PI and their later predominance at 59 h PI.

3.4. Dose dependent cell impedimetric response

We tested the capabilities of our system as a *C. parvum* infectivity sensor. Inoculation with inactivated oocysts as described before produced no infectious forms whereas pristine ones do. We therefore postulate one can produce sample of various infectivities by mixing pristine and inactivated oocysts. For this purpose, we compared the impedimetric reponses of four [sporozoite]:[cultivated cell] ratios, i.e. 1 sporozoite for 1, 2 or 4 cells (referred as 1:1, 1:2 and 1:4) and 1 freeze-and-thaw inactivated sporozoite per cell (0:1, negative control). Fig. 6A shows the normalized impedance at a frequency of 30 kHz ($|Z(t,30\ khz)|_{norm}$), which was determined as the most sensitive for a sensor application (Fig. S5).

The 3 stages previously described can be seen for each [viable sporozoite]:[cultivated cell] ratio. The peaks of impedance observed during the second stage were relatively synchronous between the three ratios (Table S2) and their difference of amplitude can therefore conveniently be plotted as shown in Fig. 6B. Furthermore, the beginning of the third stage depends on the inoculum, as it starts at 40 h PI, 44 h PI and 55 h PI respectively for the 1:1, 1:2 and 1:4 ratios.

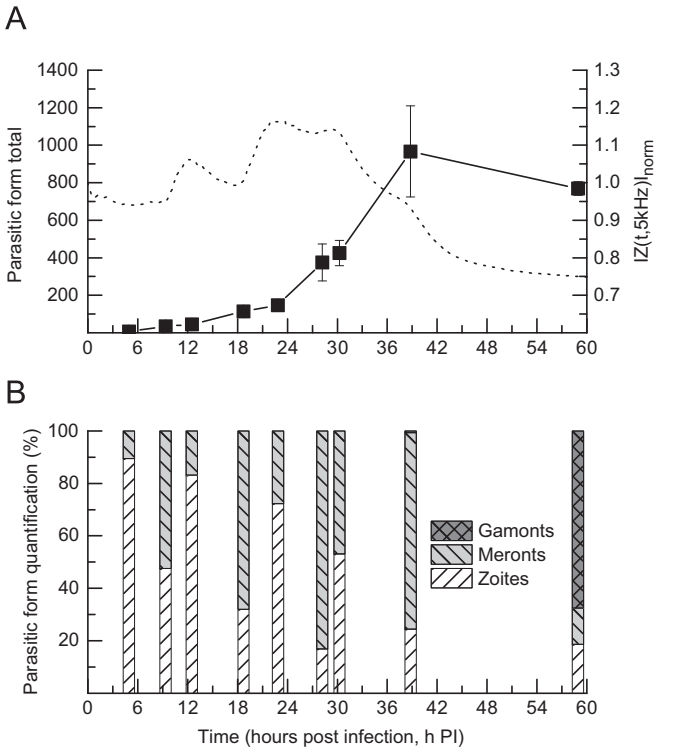

Fig. 5. Quantification of parasite stage and infection progression according to impedance variations. (A) Total parasitic forms counted in 9 frames for each of the 3 replicates samples (mean). Normalized impedance recorded for the 1:1 [viable sporozoite]:[cultivated cell] ratio. (B) Average number of parasitic forms converted into a percentage of the total parasite detected per time point.

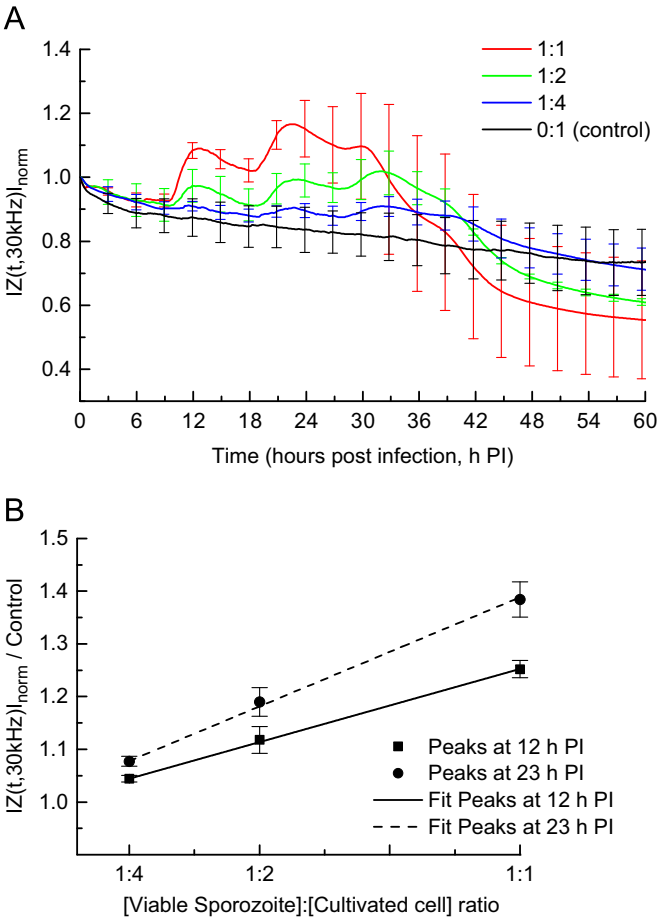

Fig. 6. Dose response of HCT-8 cells infected by *Cryptosporidium parvum*. (A) Time-course measurement of normalized impedance at 30 kHz $|Z(t,30\text{ khz})|_{norm}$ for various [viable sporozoite]:[cultivated cell] ratios. The negative control 0:1 corresponds to sporozoites inactivated by a freezing-and-thawing step. Values are mean ± SD, $n=3$. (B) Linear relationship between normalized impedance magnitude peaks (divided by the control=1) at 12 h PI and 23 h PI and the [viable sporozoite]:[cultivated cell] ratio. Equations of fit are $y=ax+b$ with, for Peaks at 12 h PI: $a=0.27777\pm0.00410$ and $b=0.97478\pm0.00175$ ($r^2=0.99956$) and for Peaks at 23 h PI: $a=0.41419\pm0.01536$ and $b=0.41419\pm0.01536$ ($r^2=0.99725$).

4. Discussion

We showed that the temporal evolution of the host cell impedimetric reponse to *C. parvum* infection presents 3 stages. By using an equivalent circuit, it is possible to study which components produce the changes in the spectra during these stages and thus postulate plausible biological mechanisms. Fitting the data with our equivalent circuit indicates that the variation values of n_{trans} and P_{trans} related to the cells themselves and R_{para} to the paracellular space encapsulate most of the time evolution of the system. In a CPE, the factor n is closely related to the "non-ideal" behavior of the CPE compared to a capacitor (Cole and Cole, 1941), as it can be regarded as a distribution parameter for time constants (Grimnes and Martinsen, 2000). The decrease of n_{trans} during the progression of the infection can therefore be related to the increase of heterogeneity of the cells in terms of size and shape (Foster and Schwan, 1989; Ivorra et al., 2005) as some are infected and some not. The final decrease of P_{trans}, magnitude of a more capacitive element, can be attributed to the decrease of cell coverage observed at the end of the experiment (Fig. S6), which reduces the electrode effective area (McAdams et al., 1996). Most of the impedance evolution however is linked to the variation of R_{para}.

To better understand the underlying biological mechanisms governing this response, we performed thorough parasite counting and classification at key moments of the infection, as determined by the impedimetric response. The results obtained are in good agreement with previous reports concerning *Cryptosporidium* life cycle, in which a majority of zoites was observed at 6 h PI (Borowski et al., 2010; Mauzy et al., 2012) and first multinuclear forms were described after 12 h PI (Mauzy et al., 2012; Slifko et al., 1997). Our observation confirmed that initial parasitic development was supported by asexual reproduction with a predominance of zoites or meronts until at least 30 h PI. Whereas Mauzy revealed a single transition from zoite to meront predominance in the early development of *C. parvum* with arbitrary sampling times (Mauzy et al., 2012), we show for the first time multiple alternations of form predominances. Indeed, during the first 30 h of the infection, meronts (proliferating forms) liberate zoites (infective forms) between local minima and peaks while zoites develop to meronts between peaks and local minima. The real-time impedimetric response gives us as well the transition kinetics between zoite predominances from 7 h to 13 h (see Table S2), an information never obtained before.

Based on this information and the knowledge of the systems, we now turn to link the impedimetric response to the underlying biology. The decrease of R_{para} could be explained by the destruction of the cells or by an increase of the permeability of their intercellular junctions. Fig. S6 shows that the cell coverage is constant during the 0–24 h PI period thus contradicting the first hypothesis. By contrast, as the parasitic load increases later on and concomitantly with the first sexual forms we observe in our samples, we measure a significant decrease of the cell coverage which leads to a R_{para} decrease in our fit.

Since cell layer degradation is not the main cause for R_{para} variation in the first 24 h, intercellular junctions related phenomena must be investigated. According to previous works, IS

applied on cells indeed enables the study of paracellular pathways (Giaever and Keese, 1991). It was determined that during the invasion step, many infectious agent (virus, bacteria, protozoa) degrade paracellular permeability to improve their penetration in cell layers (Bonazzi and Cossart, 2011). Recent data on an enteric Apicomplexa parasite (*Giardia duodenalis*) showed that this pathogenic agent disrupts intercellular junctions, inducing a reduction of the transepithelial resistance (TEER) (Maia-Brigagão et al., 2012). Authors showed that these permeability alterations were associated to trophozoite attachment, and then more particularly to the parasite invasive processes. Such observations suggest that recorded impedance decreases could be associated to *Cryptosporidium* invasion process. Previous reports showed tight junction disruptions (Buret et al., 2003), which are linked with permeability increases, are a factor of zoite invasion and trophozoite formation, reinforcing this hypothesis.

Impedance increases seem to be related to host cell responses to *Cryptosporidium* development from meront to zoite structures. It was shown that enterocytic layers release cytokines such as TGF-β in the medium in response to infection by *C. parvum* (Maillot et al., 2000). More particularly, this molecule presents a protective effect in the intestinal barrier by a reduction of the paracellular permeability through tight junction associated pathways (Howe et al., 2005). The TGF-β production would therefore explain the impedance increases, as seen in the works of Roche et al. (2000) and the review of Suzuki (2013), observed in our work associated to major meront forms as a cell layer response to infection. We therefore believe that impedance variations during *Cryptosporidium* infections are a consequence of parasite invasion and cell layer response, which would respectively induce disruption or reinforcement of tight junctions.

Then, we want to assess and quantify the ability of our system to act as an infectivity sensor for *C. parvum*. Fig. 6A shows peaks visible at 12 h PI and 23 h PI, which are correlated to the viable parasite dose (Fig. 6B). In fact, plotting the amplitude of the peaks with respect to the control as a function of [viable sporozoite]: [cultivated cell] ratio shows a clear monotonous increase. A first order interpretation of this dose response shows that the second peak yields a better sensitivity (slope 0.41 Ω/ratio) and a better limit of detection than the first one. This indicates that the impedance of the cell layer is affected by the parasite action early on in the infection as early as 10 h ($p < 0.05$). These detection times are at least 6 times faster than current techniques (neonatal mice: ±6 days; cultivated cell with IFA: ±48−72 h (Johnson et al., 2012)).

5. Conclusion

We created an impedance-based sensor to continuously follow for the first time cell response to protozoan parasite infection. Compared to current analysis techniques in quantitative monitoring of infection processes which require to fix and label the infected cells, our real-time non-invasive monitoring allows us to define meaningful sampling times for further analyses. In this study, this approach made it possible to detect the homogenous manner in which the parasite early development unfolds. Furthermore, we have demonstrated its application as a protozoan infectivity sensor, which responds faster than current methods. Improving parasite transport to the sensing layer by microfluidics and miniaturizing the sensing surface could improve sensitivity and thus opens opportunities for high-throughput and automatized infectivity tests.

Acknowledgments

This work was funded by the Nord Pas-de-Calais region (France) and the Norbert Segard foundation. This work was also partly supported by the French RENATECH network and the Institut Supérieur de l'Electronique et du Numérique (ISEN). Besides, we thank Karin Sahmer (Laboratoire Génie Civil et Géo-Environnement (LGCGE), Institut Supérieur d'Agriculture, F-59046, Lille, France) for her help regarding the ANOVA analysis.

Appendix A. Suplementary Information

Supplementary data associated with this article can be found in the online version at.
http://dx.doi.org/10.1016/j.bios.2014.11.009.

References

Arndt, S., Seebach, J., Psathaki, K., Galla, H.-J., Wegener, J., 2004. Biosens. Bioelectron. 19, 583–594.
Atienza, J.M., Zhu, J., Wang, X., Xu, X., Abassi, Y., 2005. J. Biomol. Screen. 10, 795–805.
Bagnaninchi, P.O., Drummond, N., 2011. Proc. Natl. Acad. Sci. 108, 6462–6467.
Baldursson, S., Karanis, P., 2011. Water Res. 45, 6603–6614.
Bonazzi, M., Cossart, P., 2011. J. Cell Biol. 195, 349–358.
Borowski, H., Thompson, R.C.A., Armstrong, T., Clode, P.L., 2010. Parasitology 137, 13–26.
Buret, A.G., Chin, A.C., Scott, K.G., 2003. Int. J. Parasitol. 33, 1363–1371.
Cacciò, S.M., Pozio, E., 2006. Expert Rev. Anti Infect. Ther. 4, 429–443.
Certad, G., Ngouanesavanh, T., Guyot, K., Gantois, N., Chassat, T., Mouray, A., Fleurisse, L., Pinon, A., Cailliez, J.-C., Dei-Cas, E., Creusy, C., 2007. Infect. Agents Cancer 2, 22.
Chalmers, R.M., 2012. Ann. Dell Isit. Super. Sanità 48, 429–446.
Chappell, C.L., Okhuysen, P.C., Langer-Curry, R., Widmer, G., Akiyoshi, D.E., Tanriverdi, S., Tzipori, S., 2006. Am. J. Trop. Med. Hyg. 75, 851–857.
Chen, F., Huang, K., Qin, S., Zhao, Y., Pan, C., 2007. Vet. Parasitol. 150, 13–17.
Cole, K.S., Cole, R.H., 1941. J. Chem. Phys. 9, 341–351.
De Blasio, B.F., Laane, M., Walmann, T., Giaever, I., 2004. BioTech. 36, 650–654 (656, 658 passim).
De Levie, R., 1965. Electrochim. Acta 10, 113–130.
Ehret, R., Baumann, W., Brischwein, M., Schwinde, A., Stegbauer, K., Wolf, B., 1997. Biosens. Bioelectron. 12, 29–41.
Fayer, R., 2010. Exp. Parasitol. 124, 90–97.
Foster, K.R., Schwan, H.P., 1989. Crit. Rev. Biomed. Eng. 17, 25–104.
Giaever, I., Keese, C.R., 1984. Proc. Natl. Acad. Sci. 81, 3761–3764.
Giaever, I., Keese, C.R., 1991. Proc. Natl. Acad. Sci. U.S.A. 88, 7896–7900.
Grimnes, S., Martinsen, ØG., 2000. Bioimpedance and Bioelectricity Basics. Academic Press, New York, NY, USA.
Hijjawi, N.S., Meloni, B.P., Morgan, U.M., Thompson, R.C.A., 2001. Int. J. Parasitol. 31, 1048–1055.
Houssin, T., Follet, J., Follet, A., Dei-Cas, E., Senez, V., 2010. Biosens. Bioelectron. 25, 1122–1129.
Howe, K.L., Reardon, C., Wang, A., Nazli, A., McKay, D.M., 2005. Am. J. Pathol. 167, 1587–1597.
Ivorra, A., Genescà, M., Sola, A., Palacios, L., Villa, R., Hotter, G., Aguiló, J., 2005. Physiol. Meas. 26, S165.
Johnson, A.M., Giovanni, G.D.D., Rochelle, P.A., 2012. Appl. Environ. Microbiol. 78, 156–162.
Jorcin, J.-B., Orazem, M.E., Pébère, N., Tribollet, B., 2006. Electrochim. Acta 51, 1473–1479.
Keegan, A.R., Fanok, S., Monis, P.T., Saint, C.P., 2003. Appl. Environ. Microbiol. 69, 2505–2511.
King, B.J., Keegan, A.R., Phillips, R., Fanok, S., Monis, P.T., 2012. Parasitology 139, 1533–1546.
Mac Kenzie, W.R., Hoxie, N.J., Proctor, M.E., Gradus, M.S., Blair, K.A., Peterson, D.E., Kazmierczak, J.J., Addiss, D.G., Fox, K.R., Rose, J.B., Davis, J.P., 1994. N. Engl. J. Med. 331, 161–167.
Maia-Brigagão, C., Morgado-Díaz, J.A., De Souza, W., 2012. Parasitol. Int. 61, 280–287.
Maillot, C., Gargala, G., Delaunay, A., Ducrotte, P., Brasseur, P., Ballet, J.J., Favennec, L., 2000. Parasitol. Res. 86, 947–949.
Mauzy, M.J., Enomoto, S., Lancto, C.A., Abrahamsen, M.S., Rutherford, M.S., 2012. PLoS One 7, e31715.
McAdams, E.T., Jossinet, J., Lackermeier, A., Risacher, F., 1996. Med. Biol. Eng. Comput. 34, 397–408.
McAdams, E.T., Lackermeier, A., McLaughlin, J.A., Macken, D., Jossinet, J., 1995. Biosens. Bioelectron. 10, 67–74.

Meissner, R., Eker, B., Kasi, H., Bertsch, A., Renaud, P., 2011. Lab Chip 11, 2352–2361.
Okhuysen, P.C., Chappell, C.L., Crabb, J.H., Sterling, C.R., DuPont, H.L., 1999. J. Infect. Dis. 180, 1275–1281.
Pomerantsev, A.L., 2005. Progress in Chemometrics Research. Nova Publishers, New York, NY, USA.
Roche, J.K., Martins, C.A.P., Cosme, R., Fayer, R., Guerrant, R.L., 2000. Infect. Immun. 68, 5635–5644.
Schwan, H.P., 1985. IEEE Trans. Electr. Insul. EI-20, 913–922.
Slifko, T.R., Friedman, D., Rose, J.B., Jakubowski, W., 1997. Appl. Environ. Microbiol. 63, 3669–3675.
Snelling, W.J., Xiao, L., Ortega-Pierres, G., Lowery, C.J., Moore, J.E., Rao, J.R., Smyth, S., Millar, B.C., Rooney, P.J., Matsuda, M., Kenny, F., Xu, J., Dooley, J.S.G., 2007. J. Infect. Dev. Ctries. 1, 242–256.
Solly, K., Wang, X., Xu, X., Strulovici, B., Zheng, W., 2004. ASSAY Drug Dev. Technol. 2, 363–372.
Spegel, C., Heiskanen, A., Skjolding, L.H.D., Emnéus, J., 2008. Electroanalysis 20, 680–702.
Suzuki, T., 2013. Cell. Mol. Life Sci. 70, 631–659.
Upton, S.J., Tilley, M., Brillhart, D.B., 1994. FEMS Microbiol. Lett. 118, 233–236.
Ussing, H.H., Zerahn, K., 1951. Acta Physiol. Scand. 23, 110–127.
Wang, L., Zhu, J., Deng, C., Xing, W., Cheng, J., 2008. Lab Chip 8, 872–878.
Wegener, J., Abrams, D., Willenbrink, W., Galla, H.-J., Janshoff, A., 2004. BioTech. 37 (590), 592–594 (596–597).
Wegener, J., Keese, C.R., Giaever, I., 2000. Exp. Cell Res. 259, 158–166.